remote sensing

MDPI

Article

Classifying Sub-Parcel Grassland Management Practices by Optical and Microwave Remote Sensing

Mathilde De Vroey *, Julien Radoux and Pierre Defourny

Earth and Life Institute, Université Catholique De Louvain, 1348 Louvain-la-Neuve, Belgium
* Correspondence: mathilde.devroey@uclouvain.be

Abstract: Grassland management practices and intensities are key factors influencing the quality and balance of their provisioning and regulating ecosystem services. Most European temperate grasslands are exploited through mowing, grazing, or a combination of both in relatively small management units. Grazing and mowing can however not be considered equivalent because the first is gradual and selective and the second is not. In this study, the aim is to differentiate grasslands in terms of management practices and to retrieve homogeneous management units. Grasslands are classified hierarchically, first through a pixel-based supervised classification to differentiate grazed pastures from mown hay meadows and then through an object-based mowing detection method to retrieve the timing and frequency of mowing events. A large field dataset was used to calibrate and validate the method. For the classification, 18 different input feature combinations derived from Sentinel-1 and Sentinel-2 were tested for a random forest classifier through a cross-validation scheme. The best results were obtained based on the Leaf Area Index (LAI) times series with cubic spline interpolation. The classification differentiated pastures (grazed) from hay meadows (mown) with an overall accuracy of 88%. The classification is then combined with the existing parcel delineation and high-resolution ancillary data to retrieve the homogeneous management units, which are used for the object-based mowing detection based on the Sentinel-1 coherence and Sentinel-2 NDVI. The mowing detection performances were increased thanks to the grassland mask, the management unit delineation, and the exclusion of pastures, reaching a precision of 93% and a detection rate of 82%. This hierarchical grassland classification approach allowed to differentiate three types of grasslands, namely pastures, and meadows (including mixed practices) with an early first mowing event and with a late first mowing event, with an overall accuracy of 79%. The grasslands could be further differentiated by mowing frequency, resulting in five final classes.

Keywords: grasslands; management; grazing; mowing; Sentinel-1; Sentinel-2

Citation: De Vroey, M.; Radoux, J.; Defourny, P. Classifying Sub-Parcel Grassland Management Practices by Optical and Microwave Remote Sensing. *Remote Sens.* **2023**, *15*, 181. https://doi.org/10.3390/rs15010181

Academic Editor: Giuseppe Modica

Received: 26 October 2022
Revised: 16 December 2022
Accepted: 24 December 2022
Published: 29 December 2022

1. Introduction

Grasslands cover about one-third of the global ice-free land surface. In Europe, they account for approximately one-third of the utilized agricultural area. Grasslands are a key element of our agricultural systems as they provide nearly half of the feed requirements for global livestock production [1,2]. They also play an essential role in regulating, e.g., soil erosion, carbon, water, and nitrogen fluxes [3–5] and are habitats for a broad range of plant and animal species [6,7].

In land-cover maps, grasslands and other open biotopes are often embedded in one broad land-cover class (e.g., [8–10]). However, the quality and quantity of—and the synergies and trade-offs between—their provisioning and regulating ecosystem services vary significantly depending on the grassland types, grassland-use intensity, and environmental context [11–13]. More specifically, grasslands-use intensity has a significant impact on their ecological value as habitats [13–18]. Furthermore, the spatial and temporal distribution of grassland-use intensity affects the biodiversity at the landscape scale [19,20]. It is therefore

crucial to map and monitor grassland-use intensity to further study links and balance trade-offs with their ecosystem services and their ecological value as habitats.

Most grasslands in temperate areas are managed through grazing, mechanical mowing, or a combination of both for forage production. The stocking rate of grazing animals and the timing and frequency of mowing events are major factors of grassland-use intensity. The type and quantity of management practices are commonly used as indicators to classify grasslands, both from an agricultural and an ecological perspective [21–23].

In recent years, with the emergence of new satellites combining a high spatial and temporal resolution, such as the Sentinel missions, an increasing number of studies have shown the potential of remote sensing for grassland mapping and monitoring [24,25]. Optical and radar image time series are increasingly used to discriminate grasslands habitats [26–28] or management practices [29]. A large number of studies focus on mapping grassland-use intensity either through image classification methods [30] or by retrieving different factors of grassland-use intensity (e.g., mowing frequency, grazing intensity, and/or biomass production) from image time series and auxiliary data [29,31–34]. In this context, the most frequently used index seems to be the Normalized Difference Vegetation Index (NDVI), followed by biophysical indices, such as the Leaf Area Index (LAI).

Lately, particular attention has been given to the detection of mowing events based on satellite image time series. The timing and frequency of mowing events have a great influence on grasslands provisioning and regulating ecosystem services and on biodiversity [35,36]. Several types of approaches have been explored. A majority of studies use optical imagery (e.g., Sentinel-2, Landsat, MODIS, and RapidEye), detecting mowing events through significant decreases in the NDVI, LAI, or other vegetation indices [33,37,38]. In radar remote sensing (e.g., Sentinel-1), mowing events can be detected through sudden increases in interferometric coherence time series [39,40]. Optical imagery allows detecting mowing events with more precision (i.e., less false positives) but with a lower detection rate than radar because persistent cloud cover prevents the detection of some events. A few studies, therefore, combined both optical and radar imagery, increasing the detection rate while limiting the number of false positives. Studies combining Sentinel-1 and Sentinel-2 time series for either rule-based or deep learning mowing detection methods reached high performances, with F1-scores between 79% and 84% [41,42].

Many mowing detection methods described in the literature are object based, relying on existing delineations of parcel boundaries or a preliminary segmentation step [32,39–43]. This allows a spatial smoothing of the satellite signal and avoids the salt-and-pepper effect that is inherent to pixel-based approaches [37,38,44]. One of the major drawbacks of object-based approaches is, however, the potential heterogeneity of practices inside declared or delineated parcels. When only one part of a parcel is mown at a given time and the other is grazed or mown at a different time, the signal change can be smoothed out, causing omissions.

While many studies focused on mowing detection, few have investigated the possibility of monitoring grazing activities [30,32,45] and even fewer discriminate grazed and mown grasslands [29]. Grazing has been identified as a major confounding factor to mowing detection in several studies as many false mowing detections occur in pastures [40,44] because they both result in biomass removal. However, both from an agricultural and an ecological point of view, grazing and mowing cannot be considered equivalent management practices because the first is selective (depending on the type of livestock), while the second is not.

The objective of this study is to differentiate grasslands in terms of management practices at the sub-parcel level, corresponding to homogeneous management units. Grasslands are differentiated in two hierarchical steps, combining a pixel-based and an object-based method to account for the variability in the practices inside declared parcels.

The first step consists of detecting the main management practice at the pixel level to differentiate pastures, managed exclusively through grazing, from hay meadows, which are mown mechanically. This preliminary pixel-based classification approach tackles two

main issues in grassland monitoring, namely (i) the heterogeneity of practices inside declared parcels and (ii) grazing as a confounding factor for mowing detection.

Then, an object-based mowing detection method based on the Sentinel-1 (S1) and Sentinel-2 (S2) time series is applied to the management units classified as hay meadows to further differentiate them and to produce an exhaustive grassland management practice classification.

2. Materials

2.1. Study Area

This study was performed on permanent grasslands in Wallonia, the southern region of Belgium (Figure 1). Wallonia covers 16 901 km^2 and around 35% of its utilized agricultural area is occupied by permanent grasslands [46]. The majority of permanent grasslands are managed through relatively intensive mowing, grazing, or a combination of both. Extensive hay meadows which are exclusively mown are uncommon. In most agricultural grasslands, exploitation (grazing or mowing) starts in mid-April. In grasslands of high biological interest, supported by the European (EU) Common Agricultural Policy (CAP), mowing is only allowed after the 15th of June and before the 31th of October for flowering purposes.

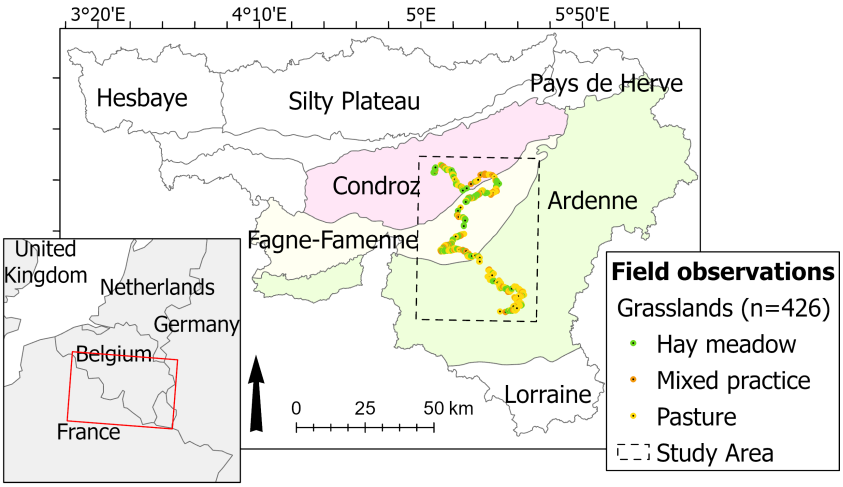

Figure 1. Extent of the study area (Wallonia, Belgium) and location of grassland parcels observed during the field campaign. Orthophoto credits: Service Public de Wallonie (SPW).

2.2. Satellite Data

The grassland classification method developed in this study is based on Sentinel-1 Synthetic Aperture Radar (SAR) and Sentinel-2 multi-spectral optical time series. All S1 and S2 scenes covering the study area during the study period (April 9 to July 19 2019) were downloaded from Copernicus Open Access Hub.

During the study period, 17 scenes were acquired by Sentinel-1 A and B in ascending pass and 18 in descending pass over the study area (Table 1). All scenes were processed from Single-Look Complex to Ground Range-Detected γ_0 backscattering amplitudes, using SNAP Sentinel-1 toolbox [47]. Processing steps include calibration, georeferencing, deburst, and terrain correction. The S1 γ_0 images were resampled from 15 m to 10 m, using the nearest-neighbour method, to match the pixel size of the S2 images. Sentinel-2 A and B acquired 17 multi-spectral images with less than 80% cloud cover over the study area (tile 31UFR) during the study period (April 9 to July 19, 2019). The top-of-atmosphere images (Level 1) were converted to surface reflectances (Level 2) using Sen2Cor v2.10 for atmospheric correction. The function of mask (Fmask) method [48] was used for cloud masking because it was shown to be more accurate than the Sen2Cor cloud masking method [49].

Table 1. Sentinel-1 and 2 images acquired during the study period (April 9 to July 19, 2019) and used to compute the classification features.

Mission	Max Cloud Cover	Pass (S1)/Tile (S2)	n Acquisitions	Features
Sentinel-1	-	ascending descending	17 18	VV_{asc}, VV_{desc}, VH_{asc}, VH_{desc}, $ratio_{asc}$, $ratio_{desc}$
Sentinel-2	80%	31UFR	17	$NDVI_{linear}$, $NDVI_{spline}$, $CIre_{linear}$, $CIre_{spline}$, LAI_{linear}, LAI_{spline}

2.3. Field Data

The reference data used for training and validation were obtained through a field campaign across 3 agroecological regions of Wallonia (Condroz, Fagne-Famenne, and Ardenne) in 2019. Between the 9th of April and the 19th of July 2019, the management practices of 426 permanent grassland parcels were monitored through a windshield survey (Figure 1). Each parcel was visited 11 times during the study period. The field visits were carried out with intervals of 6, 12, or 18 days, with the highest frequency in May and June when the first cuts are expected to occur and the regrowth would be relatively fast. On each visit, the management status of each grassland parcel was recorded ('growing', 'recently cut', 'being cut', 'grazed'). Based on the observations, four classes of grasslands could be differentiated: parcels where only grazing was observed (pastures, n = 201), grazed parcels with at least one mowing event (mixed practices, n = 61), and parcels with no grazing but at least one mowing event before (hay meadows (<15/06), n = 78) or after June 15th (extensive hay meadows ($\geq$15/06), n = 76). On 11 parcels, the management practice could not be defined with certainty based on the field observations. These parcels were discarded from the reference dataset.

3. Methodology

Previous studies have shown the great potential of combining Sentinel-1 and Sentinel-2 for grassland mowing detection. Because of the speckle inherent to SAR imagery, pixel-based approaches are challenging. Therefore, studies using SAR data for mowing detection rely on object-based approaches, averaging the signal per parcel.

However, grassland parcels, as declared by farmers in the Land Parcel Identification System (LPIS, i.e., a vector dataset based on legal declarations by farmers in each EU country, including parcel boundaries and crop types), often include several management units that are not all exploited at the same time or in the same way. To illustrate, Figure 2 shows the Sentinel-2-derived LAI time series of a grassland parcel in our study area. The parcel's average time series (in gray) is relatively constant, while about half of the pixel time series (in green) significantly decreases in the middle of June. This decrease in LAI is due to a mowing event that occurred on one part of the declared parcel, while the other part was not mown but grazed. The two management units are also visible on the orthophoto (dashed red line in Figure 2).

This is an issue for object-based grassland monitoring methods, such as the one developed in Sentinels for Common Agricultural Policy (Sen4CAP) [42]. Therefore, we develop a hierarchical grassland characterization approach combining a pixel-based classification method and an object-based mowing detection method.

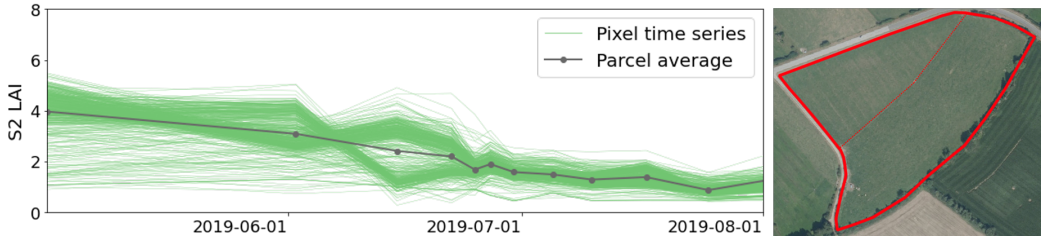

Figure 2. Leaf Area Index (LAI) time series (retrieved from Sentinel-2) extracted per pixel and per parcel (average value) for a grassland parcel (drawn in red on the orthophoto (SPW)). The dashed red line shows the boundary of the management units.

3.1. Pixel-Based Supervised Classification

In this phase, the aim is to differentiate grasslands in terms of main management practice (grazing or mowing) and retrieve homogeneously managed parcels for further characterization. A pixel-based supervised classification method is used to discriminate exclusively grazed *pastures* from mown *hay meadows*. The *hay meadows* class includes mixed practices, which are alternatively mown and grazed. Field observations were used to build a reference dataset to train and validate a random forest classifier based on S2 and S1 time series.

3.1.1. Input Features

Vegetation indices derived from specific spectral bands are commonly used to emphasize certain properties of a vegetation cover, such as biomass. We made the hypothesis that grasslands that are grazed throughout the season should have relatively constant and stable vegetation index time series compared to grasslands with at least one mowing event causing a sudden change in biomass [38,44]. To test the sensitivity of the classification to the choice of vegetation index, three spectral vegetation indices and one biophysical index derived from Sentinel-2 were considered for the classification, namely NDVI, the red-edge chlorophyll index (CIre), and the LAI. The NDVI is computed as the normalized difference between the near-infrared (band 8) and the red (band 4) reflectance (Equation (1)) and is largely used for vegetation monitoring and more specifically for grassland mapping and mowing detection [33,37,44]. The CIre is related to the increase in reflectance between the red and near-infrared (i.e., the red edge) which is linked to biomass and chlorophyll content of vegetation. It is calculated as the ratio between lower (band 5) and upper (band 7) red-edge reflectance (Equation (2)). The CIre was used by Hardy et al. [34] to retrieve grassland biomass.

$$NDVI = \frac{Band\,8 - Band\,4}{Band\,8 + Band\,4} \quad (1)$$

$$CIre = \frac{Band\,7}{Band\,5} - 1 \quad (2)$$

The LAI was retrieved from Sentinel-2 reflectances through the calibrated artificial neural network from the BV-NET tool [50], which is implemented in several European Space Agency (ESA) agricultural monitoring toolboxes (e.g., Sen2Agri, Sen4CAP).

To fill gaps due to cloud cover, the S2 vegetation index time series were temporally interpolated using the Image Time-Series Gap Filling tool [51] available in Orfeo Toolbox [52]. As we intend to apply this classification to a larger area, the time series were temporally resampled to a 5-day grid, starting at the first acquisition date, to overcome the multiple-day offset between adjacent satellite tracks [53]. Both linear and cubic spline interpolations were tested for the three indices. A total of 6 different S2 feature sets were thereby tested as input features for the random forest classifier (Table 1).

Microwave data guarantee regular temporal coverage and can provide complementary information to optical data. The complementarity of Sentinel-1 and Sentinel-2 was shown in the context of grassland mowing detection [41,42]. Therefore, we tested the classification with microwave time series alone and in combination with Sentinel-2 data. Sentinel-1 γ_0

backscattering amplitudes in VV and VH polarization and the ratio VV/VH were used as input features. Ascending and descending pass acquisitions were made at different times of the day and with different look angles. Because radar signal is strongly impacted by water content, morning acquisitions are significantly affected by dew and vegetation water content. Each polarization was therefore tested in ascending (e.g., VV_{asc}) and descending (e.g., VV_{desc}) pass separately. A total of 6 different S1 feature sets were thereby tested as input for the classification (Table 1).

In addition, to assess the complementarity of S1 and S2 for differentiating *pastures* and *hay meadows*, the best-performing S2 feature set was tested in combination with the best-performing S1 feature as well as the respective time-series minimum (*min*), maximum (*max*), mean (*mean*), and median (*median*) values and all statistics together (*stats*). A total of 6 different S1 and S2 feature combinations were thereby tested.

3.1.2. Classification Mask

The classification mask was built by combining and resampling a grassland mask and a shadow mask (Figure 3).

The grassland mask was obtained by reclassifying the 2 m resolution land-cover product of LifeWatch [54]. Two grassland classes, namely "Monospecific grassland with graminoids" and "Diversified grassland and shrubland", were taken into account.

The shadow mask was based on a digital surface model (DSM) (Figure 4). The DSM of Wallonia is a product of the orthophoto acquisition campaign of 2019 (Service Public de Wallonie, SPW). Shadow projections were computed with 2 m resolution based on the object heights from the DSM and a sun azimuth and elevation of 146°and 38°, respectively.

The combined grassland and shadow mask was resampled to 10m to match Sentinel-2 pixels. A minimum rule was applied for the resampling to take only pure pixels into account for the classification, with 100% grassland and no shadow.

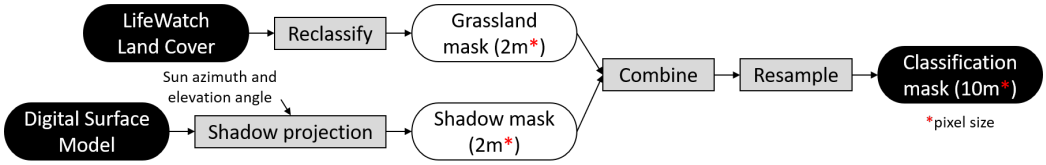

Figure 3. Classification mask flowchart. The mask was built using the two grassland classes of the LifeWatch land-cover product and shadow projections based on a digital surface model (DSM). The mask was resampled to 10m to match the pixel size of Sentinel-2.

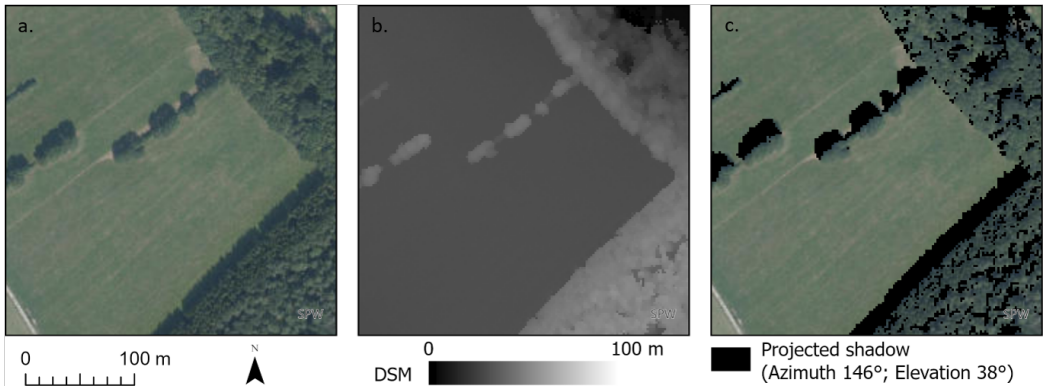

Figure 4. (**a**) Orthophoto (SPW) with tree shadows in a grassland, (**b**) digital surface model (DSM, credits SPW) showing the elevation of the top of objects above the ellipsoid, and (**c**) projected shadows based on the DSM with given sun angles.

This mask allows to classify only pure grassland pixels and discard pixels that are influenced by shadows or trees (Figure 5). The LAI time series of masked pixels (in gray on Figure 5) consistently differ from the valid pixels (in green on Figure 5). The majority of

masked pixels in this example are mostly influenced by shadow, which manifests in lower LAI values throughout the season. A few masked pixels are influenced mostly by trees and shrubs and have higher LAI values compared to valid grassland pixels.

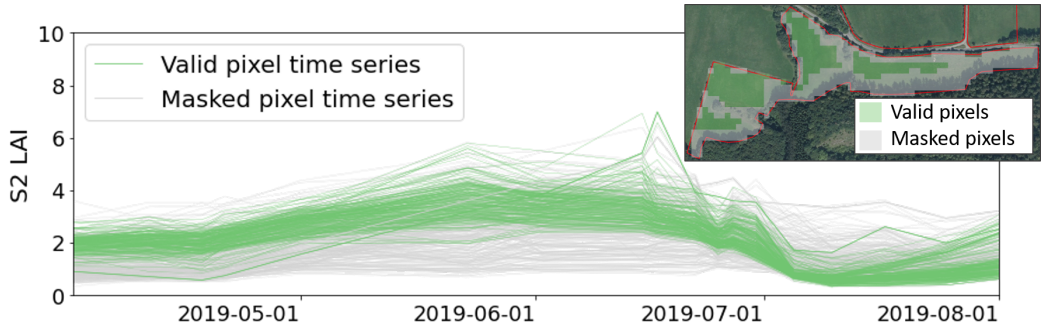

Figure 5. Leaf Area Index (LAI) time series (retrieved from Sentinel-2) extracted per valid (green) and masked (gray) pixel for a grassland parcel (drawn in red on the orthophoto (SPW)).

3.1.3. Reference Data

Based on the field observations, the observed parcels could be classified into two categories: *pastures*, which were exclusively grazed during the study period, and *hay meadows* on which at least one mowing event was observed. The reference parcels were redrawn manually, based on the LPIS, the grassland mask, and the Walloon orthophoto of 2019 (SPW) to obtain homogeneous reference parcels. When two or more management units could be differentiated inside one declared parcel, only the management units closest to the road were considered to be matching the field observation.

During the redrawing, 5 parcels were discarded because they contained no valid pixels due to shadow. In total, the reference dataset contained 412 parcels (194 *pastures* and 218 *hay meadows*). They were equally partitioned into a training and a validation dataset through stratified random sampling. The training dataset was used to train, calibrate, and compare the classification methods through cross-validation. The validation dataset was used to validate the final product.

3.1.4. Cross-Validation

Different classifiers were evaluated and compared through a 4-fold cross-validation scheme. The training dataset was split into 4 subsets to keep a reasonable number of samples for the validation at each iteration. The classifiers were compared based on the mean overall accuracy (OA) and its standard deviation. The best-performing classifier was then trained using the whole training dataset. The resulting classification was then validated with the validation dataset. The user and producer accuracy (UA and PA) of both classes were also computed in addition to the overall accuracy.

Both during the cross-validation and the final validation, we applied a per-pixel wall-to-wall validation, assessing each pixel inside each redrawn homogeneous reference parcel.

3.2. Object-Based Mowing Detection

The pixel-based classification obtained in the first step was used in combination with the LPIS to obtain homogeneous parcels for an object-based mowing detection using the Sen4CAP toolbox v3.0 [55].

3.2.1. Classification Post-Processing

The following steps were applied to obtain homogeneous management unit polygons based on the classification and the LPIS.

1. The classification is filtered to remove isolated pixels: a pixel value is changed to the other class if there are less than 4 pixels of the same class in a 3×3 window around the pixel.

2. All parcels declared as grasslands (temporary or permanent) are extracted from the LPIS.
3. The LPIS grassland polygons are rasterized at 10 m resolution using the parcel unique feature IDs (between 1 and 999,999) as raster values.
4. The binary classification is multiplied by 10^6 and summed up to the values rasterized LPIS. This combined raster carries information about the management class (*pastures* vs. *hay meadows*) and the LPIS parcel delineation.
5. The combined raster is polygonized.
6. No-data polygons (i.e., covering masked areas) and polygons with an area smaller than 1000 m^2 (10 pixels) are discarded.

3.2.2. Mowing Detection Method

The mowing detection method of Sen4CAP is based on two separate algorithms detecting changes in Sentinel-2 and Sentinel-1 time series extracted per parcel (Figure 6). The detailed method is described in De Vroey et al. [42].

The S1 algorithm detects significant increases in VH interferometric coherence by comparing each value $coh(t)$ to the previous value $coh\_fit(t-1)$ obtained by linear fit of the six previous values $[coh(t-6), ..., coh(t-1)]$. The detection is based on a Constant False Alarm Rate (CFAR) adaptive threshold ($3.0 \times 10^{-7} \times \sigma$) that takes into account the standard deviation of the residual fitting errors (σ). The S2 algorithm detects a mowing event when the decrease in NDVI between two consecutive cloud-free acquisitions is larger than a given threshold, fixed at 0.12 for this region [42].

A confidence level is computed for each detection, with lower values for S1 than for S2 to compensate for the lower precision of S1 mowing detection. For each parcel, the four most confident detections are retained. For each detection, the detection interval is given along with the confidence level and the data source (S1, S2, or both). The confidence levels of the detections range from 0 to 1 and are well correlated to the precision of the detections [42].

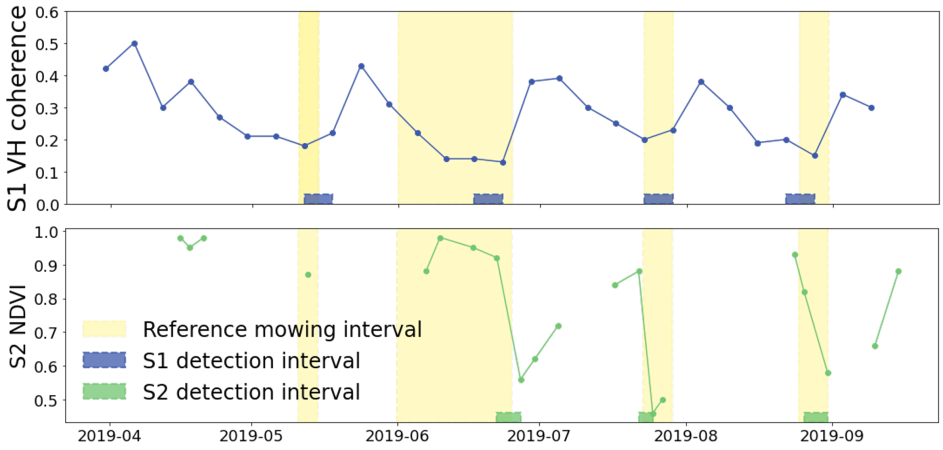

Figure 6. Illustration of the mowing detection algorithms of the Sen4CAP toolbox, based on Sentinel-1 VH coherence and Sentinel-2 NDVI time series extracted on a permanent grassland parcel.

3.2.3. Validation

The mowing detection performances were assessed at two levels. First, the actual detection of each single mowing event was validated. Second, the further classification of hay meadows, based on the mowing detections, was validated.

In the first case, the mowing detections were validated by crossing the detection intervals with reference intervals. Reference mowing intervals were retrieved from the observations made during the field campaign. A reference mowing interval consists of the time interval between an observation of short grass and the previous observation of high grass. When a detection interval intersects a reference mowing interval, it is considered

as a true positive (TP). If no reference mowing interval overlaps a detection, it is a false positive (FP), and if no detection overlaps a reference mowing interval, it is counted as a false negative (FN). The remaining intervals are true negatives (TN).

Two quality metrics, namely the *precision* and the *detection rate*, are calculated using Equations (3) and (4).

$$precision = \frac{TP}{TP + FP} \tag{3}$$

$$detection\ rate = \frac{TP}{TP + FN} \tag{4}$$

In the second case, the accuracy of the differentiation between hay meadows with an early first mowing event and a late first mowing event was validated through a confusion matrix and related quality metrics (UA, PA, and OA).

The calibration reference dataset was used to define the optimal confidence level thresholds and maximize the accuracy of the management practice classification. The validation dataset was then used to assess the result.

Here as well, to stay consistent with the previous classification validation, a per-pixel wall-to-wall validation was applied.

4. Results

4.1. Classification Algorithm Calibration

The results of the random forest classifier calibration with the different feature sets are shown in Tables 2–4. For each tested feature set, the mean overall accuracy (mean OA) and its standard deviation (std OA) over the four iterations of the cross-validation scheme are given.

Table 2 shows the calibration results for the Sentinel-2 feature sets. The highest mean OA is 88.4% obtained with LAI_{spline} and the lowest is 85.7% obtained with $NDVI_{linear}$. For all three indices, the cubic spline interpolation seems to result in slightly better performances than the linear interpolation. Given the standard deviation of the OA, ranging from 2.6% to 5.3%, the differences in the OA between the feature sets are however relatively low.

Table 3 shows the calibration results for the Sentinel-1 feature sets. The highest mean OA is obtained with the VV polarization, both in the ascending (71.3%) and descending pass (68.5%). The lowest performances are obtained with the VV/VH ratio in both passes (60.3% and 57.7% OA). The performances are overall significantly lower than with the S2 features. Moreover, the standard deviations of the OA over the iterations are higher (4.6% to 8.7%), showing a higher sensitivity of the algorithm to the training dataset.

Finally, Table 4 shows the results of the combined S2 and S1 feature sets. The best-performing S2 feature time series (LAI_{spline}) was combined with the best-performing S1 feature (VV_{asc}) to test if they improve the classification performances. The last column (delta OA) shows the change in the mean OA compared to the use of the S2 LAI_{spline} time series alone. The addition of the VV_{asc} time series to LAI_{spline} improves the mean OA by 0.2%. The VV_{asc} temporal statistics all result in a small decrease in performance, from -0.1% with $max(VV_{asc})$ to -1.1% with $min(VV_{asc})$. Overall, the differences in the mean OA and std OA are extremely small compared to those of S2 LAI_{spline} alone.

The calibration results suggest that the three tested S2 vegetation index time series allow differentiating pastures from other grasslands with high accuracy. The S1 γ_0 backscattering amplitude time series however performed lower. Moreover, the combination of the S1 VV_{asc} time series or temporal statistics to S2 features did not significantly improve the classification accuracy. For a further analysis, we used the S2 LAI time series with cubic spline interpolation because it provided the highest mean OA of the S2 features.

Table 2. Classification algorithm calibration results with the Sentinel-2 features. For each feature time series, the mean overall accuracy (mean OA) and its standard deviation (std OA) over the 4 iterations of the cross-validation scheme are given.

S2 Features	Mean OA	Std OA
LAI_{spline}	88.4%	3.5%
$CIre_{spline}$	87.3%	3.0%
LAI_{linear}	87.0%	3.7%
$CIre_{linear}$	86.9%	4.8%
$NDVI_{spline}$	86.3%	2.6%
$NDVI_{linear}$	85.7%	5.3%

Table 3. Classification algorithm calibration results with the Sentinel-1 features. For each feature time series, the mean overall accuracy (mean OA) and its standard deviation (std OA) over the 4 iterations of the cross-validation scheme are given.

S1 Features	Mean OA	Std OA
VV_{asc}	71.3%	6.5%
VV_{desc}	68.5%	8.7%
VH_{desc}	67.3%	7.1%
VH_{asc}	67.0%	4.7%
$ratio_{asc}$	60.3%	4.6%
$ratio_{desc}$	57.7%	5.2%

Table 4. Classification algorithm calibration results with the combined S1 and S2 features. For each feature time series, the mean overall accuracy (mean OA) and its standard deviation (std OA) over the 4 iterations of the cross-validation scheme are given. The change in OA compared to the use of S2 LAI_{spline} (delta OA) is provided in the last column.

S2 Feature	S1 Features	Mean OA	Std OA	Delta OA
LAI_{spline} (OA = 88.4%)	VV_{asc}	88.6%	3.0%	+0.2%
	$max(VV_{asc})$	88.3%	3.6%	−0.1%
	$mean(VV_{asc})$	88.2%	3.8%	−0.3%
	$stats(VV_{asc})$	87.9%	3.0%	−0.5%
	$median(VV_{asc})$	87.6%	3.7%	−0.9%
	$min(VV_{asc})$	87.3%	4.1%	−1.1%

4.2. Classification Validation and Post-Processing

Based on the results of the calibration, a random forest classifier was trained using the whole training dataset (n = 208) and applied to the Sentinel-2 LAI time series with spline interpolation. The resulting classification is shown in Figure 7. Visually, the classification seems relatively accurate in separating *pastures* from *hay meadows*. In some parcels, there is however a salt-and-pepper effect due to the pixel-based approach. The classification was quantitatively validated using the remaining half of the reference dataset (Table 5). The overall accuracy is 88%, which is very close to the OA obtained during the calibration (88.4%). The user and producer accuracies are also high and well-balanced. The UA is 88% for both classes. The PA is 91% for the *pastures* and 85% for the *hay meadows*.

To assess the added value of masking out pixels containing non-grassland elements (e.g., trees or buildings) or shadows, the same classifier was applied using only the grassland parcels from the LPIS as a classification mask. The OA of this classification is 87%, which is 1% lower than when using high-resolution products (land cover and DSM) to build a strict classification mask. In the examples in Figure 8, the classification without the LC and shadow mask shows some commission errors due to the trees and shadows

inside the parcels, while these pixels are masked out when using high-resolution products. The impact on the OA is small because only a limited number of pixels are involved.

Table 5. Validation of the grassland management types classification. Confusion matrix, user, producer, and overall accuracy (UA, PA, and OA) between reference (ref) and predicted (pred) types.

Ref\Pred	*Pastures*	*Hay Meadows*	PA	UA
Pastures	24267	2516	91%	88%
Hay Meadows	3277	18843	85%	88%
			0A	88%

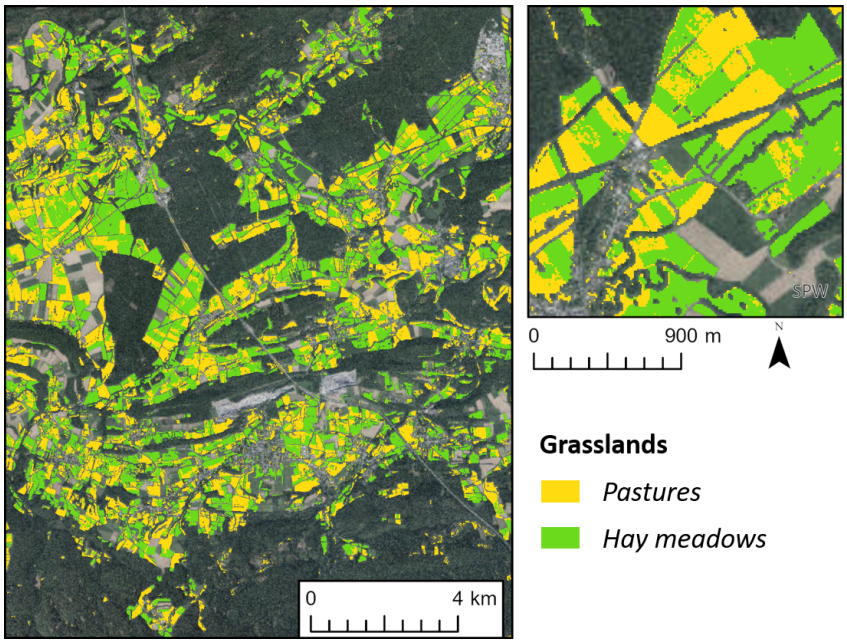

Figure 7. Pixel-based classification based on Sentinel-2 LAI time series differentiating pastures (exclusively grazed) from hay meadows (including mixed practices).

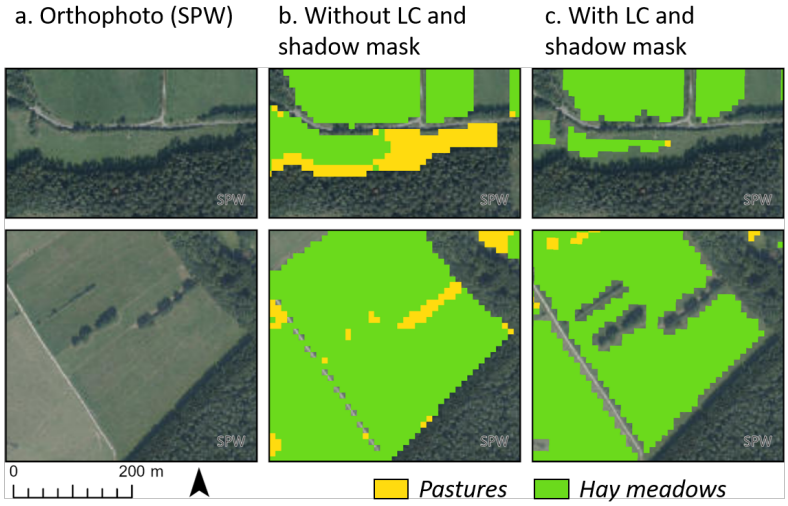

Figure 8. Comparison of the classification obtained with and without the land cover (LC) and shadow mask derived from very high resolution data.

The obtained classification was post-processed to obtain homogeneous grassland management units with a single management practice. The removal of isolated pixels (cf.

Section 3.2) allowed to significantly reduce the salt-and-pepper effect (Figure 9b). The filtered raster was then crossed with the LPIS raster and polygonized. The polygons smaller than 1000 m^2 (10 pixels) were removed to obtain clean homogeneous grassland parcels for the object-based mowing detection (Figure 9c). From the 20,796 grassland parcels declared in the LPIS in the study area, 21% contained both *pasture* and *hay meadow* management units. Furthermore, 10% of the remaining parcels contained multiple management units with the same practice (mowing or grazing). In total, 31,230 homogeneous grassland parcels were delineated through the classification in the study area.

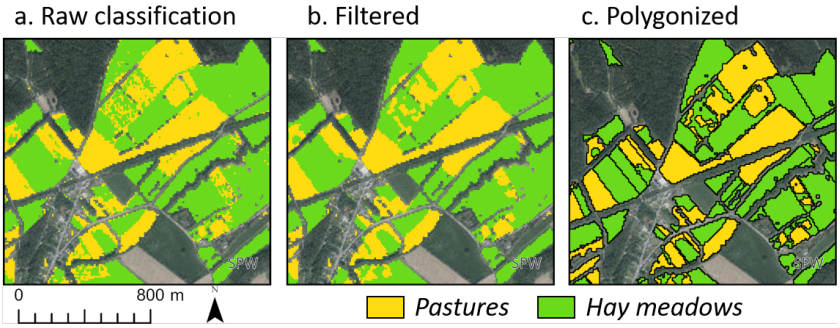

Figure 9. Post-processing of the raw classification result (**a**). Filtered to remove isolated pixels (**b**), polygonized and cleaned to remove small parcels (**c**).

4.3. Mowing Detection Calibration and Validation

The object-based grassland mowing detection method of the Sen4CAP toolbox was applied to the polygons that were classified as *hay meadows*. The mowing detections between April 9th and July 19th were validated with the reference mowing intervals from the calibration reference dataset. The obtained *precision* is 83% and the *detection rate* is 73%.

Based on the date of the first mowing event (before or after June 15th), two classes of mown grasslands could be differentiated: *early* and *late*. The confusion matrix and accuracy metrics computed with the calibration reference dataset are given in Table 6. When all the detections are taken into account (minimum confidence level ($min(conf)$) = 0.0), the OA is 61%. More than half of the *late* grasslands are incorrectly classified as *early* (PA = 45%), and the UA of the *early* grasslands is only 51%. This is due to false detections occurring before 15/06.

The confidence level was used to filter out early false positives. With a $min(conf)$ of 0.5 for the detections before 15/06 and 0.4 for the detections on or after 15/06, the PA of the *late* grasslands and the UA of the *early* grasslands are significantly higher (74% and 62%, resp.). There are more omissions of early mowing events, reducing the PA of the *early* grasslands (57%) and the UA of the *late* grasslands (75%). However, the performances are more balanced, and the overall accuracy is higher (67%). This adaptive $min(conf)$ was therefore retained for further grassland characterization.

Table 6. Calibration of the minimum mowing detection confidence level ($min(conf)$). Confusion matrices crossing the first mowing event classes (before (*early*) or after June 15th (*late*)) based on field observations (ref) and mowing detection (pred) for different $min(conf)$ of detections. The user and producer accuracies (UA and PA) are provided as well as the overall accuracy (OA).

$min(conf)$ = 0.0					$min(conf)$ = 0.5 (<15/06), 0.4 (≥15/06)				
ref\pred	*early*	*late*	no activity	**PA**	**ref\pred**	*early*	*late*	no activity	**PA**
early	6994	1262	124	**83%**	*early*	4744	3033	603	**57%**
late	6389	5545	326	**45%**	*late*	2871	9063	326	**74%**
UA	**51%**	**81%**	**OA**	**61%**	**UA**	**62%**	**75%**	**OA**	**67%**

The Sen4CAP mowing detection on the *hay meadows* (with the adaptive $min(conf)$) was finally validated with the independent validation reference dataset. The estimated

precision of the detections is 93%, and the *detection rate* is 82%. According to the validation dataset, the grasslands with *late* and *early* first mowing events were differentiated with an overall accuracy of 75%.

4.4. Hierarchical Classification of Management Practices

Based on the previous results, we can expect that the classification and mowing detection allow to hierarchically differentiate three grassland management practices with high accuracy. First, *pastures* are differentiated from *hay meadows* through the classification. Then, the *hay meadows* can be further differentiated by the first mowing date (before or after June 15th). This hierarchical classification was validated using the validation reference dataset (Table 7). The overall accuracy is 79%. The UA and PA of the *pasture* class (resp., 89% and 91%) are slightly improved compared to the raw pixel-based classification (Table 5), thanks to the post-processing. The UA and PA of the *hay meadows* with an *early* (resp., 65% and 54%) and a *late* (resp., 70% and 72%) first mowing are lower due to the confusion between both sub-classes.

Table 7. Validation of the hierarchical grassland typology. Confusion matrices crossing the main management practice classes (*pastures* and *hay meadows*) and the first mowing event classes (before (early) or after June 15th (late)) based on field observations (ref) and on the classification and mowing detection (pred). The user and producer accuracies (UA and PA) are provided as well as the overall accuracy (OA).

Ref\Pred		***Pastures***	***Hay Meadows***			**PA**
			Early	**Late**	**No Activity**	
Pastures		24224	492	1397	398	**91%**
Hay Meadows	early	1523	4846	2588	64	**54%**
	late	1587	2082	9255	0	**72%**
UA		**89%**	**65%**	**70%**	**OA**	**79%**

In addition to the first mowing date, *hay meadows* can be differentiated by the number of mowing events in the growing season. The *hay meadows* with an early first mowing (<15/06) were further split into grasslands with less than three mowing events (n < 3) and three events or more (n ≥ 3), while those with a late first mowing (≥15/06) were further split into grasslands with only one mowing event (n = 1) and two events or more (n ≥ 2). These final grassland classes are mapped in Figure 10.

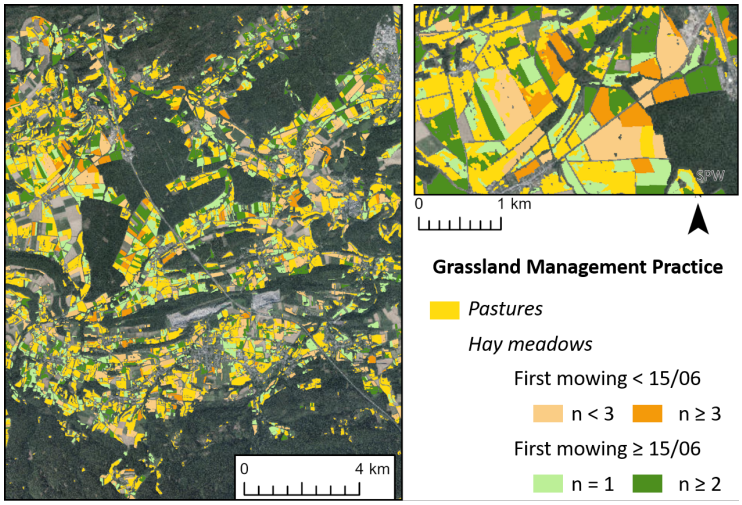

Figure 10. Grassland management practice classification. This hierarchical classification is based on the classification differentiating *pastures* from *hay meadows* and the mowing detection which further differentiates the second class by the date of the first mowing and by the number of mowing events (n).

5. Discussion

5.1. Classification and Mowing Detection Performances

One of the main motivations behind the binary classification developed in this study was to be able to exclude pastures for the subsequent mowing detection. In previous studies, grazed parcels were either not taken into account [41] or shown to be a confounding factor for mowing detection [38,42,44]. Precise information on the management practice of grasslands (i.e., mowing or grazing) is however rarely available. Using a large field dataset, we showed that this information could be retrieved with high accuracy from Sentinel-2 vegetation index time series. This corroborates the hypothesis that grazed grasslands can be distinguished from mown grasslands based on their relatively constant temporal vegetation index profiles. The LAI had already been identified as a relevant variable to discriminate grazed and mown grasslands in a study using three SPOT images [56]. The LAI retrieved from S2 with the BV-NET tool [50] was shown to be fit to the purpose of this study. It would however still need to be validated for the absolute retrieval of the LAI in temperate agricultural grasslands.

In this study, the three tested vegetation indices derived from Sentinel-2 (the NDVI, CIre, and LAI) performed similarly, and the random forest classifiers all reached a high overall accuracy. The performances obtained with the Sentinel-1 backscattering time series were much lower. This can mainly be explained by the speckle effect inherent to SAR imagery that makes a pixel-based analysis challenging without any spatial or temporal smoothing. The addition of the Sentinel-1 backscattering temporal statistics to the Sentinel-2 input features did not significantly improve the classification results. Sentinel-1 was therefore discarded for the classification step. The LAI time series with cubic spline interpolation was retained for a further analysis because it performed slightly better, but the NDVI and the CIre could be used as well because the differences in the performances were not statistically significant.

Another related aim of this pixel-based classification was to tackle the issue of grassland parcel delineation, raised in previous studies [41,42] and illustrated in Figure 2. In datasets such as the LPIS, parcel delineations often include several management units that are managed differently or at different times. The binary classification and the post-processing, including a filtering step to remove isolated pixels, allowed to retrieve more homogeneously managed grassland patches at the management units level.

Next to the heterogeneity of practices, delineated grassland parcels can also include hedges, trees, and buildings with different spectral signatures that can hinder the classification. Thanks to the 2 m resolution land-cover product that was used to build the grassland mask, the 10 m pixels with less than 100% grassland cover could be masked out. In optical remote sensing, shadows can also be a significant issue. A shadow mask, estimated through a DSM, was therefore added to the grassland mask to further optimize the classification performances. Overall, the availability of very high resolution products such as the land-cover map, the orthophoto, and the DSM was a great asset. Very high resolution data and products are increasingly available and could be used to build similar grassland masks and reproduce the classification over larger areas.

The operational object-based mowing detection method of the Sen4CAP toolbox was applied to the homogeneous patches of the *hay meadows* retrieved from the classification. According to the validation reference dataset, the method reached a *precision* of 93% and a *detection rate* of 82%. These detection performances are much higher than those obtained on the same grasslands without the preliminary classification, especially in terms of *precision*. The *precision* was only 44% when the pastures were taken into account due to false mowing detections on grazed grasslands [42]. The exclusion of pastures thanks to the classification was of course a major factor in this increased performance. However, even compared to the *precision* we obtained in De Vroey et al. [42] on hay meadows alone (73%), the present results show a significant improvement. This implies that the homogeneity of practices and the absence of trees and shadows inside the reshaped grassland parcels also contributed to the high mowing detection accuracy. In addition, the wall-to-wall pixel-based validation

applied in this study could also explain the higher performance metrics because the size of the parcels was not taken into account in the validation in the previous study [42]. The mowing detection performances obtained here are also slightly higher than those obtained with a deep learning approach combining Sentinel-1, Sentinel-2, and Landsat-8 in a convolutional neural network with a maximum *precision* of 86% and a *detection rate* of 82% [41].

While this method showed high performances in our study area in the 2019 growing season, it should be further tested in more extended areas and other seasons. For example, the effects of drought on vegetation could significantly alter the vegetation index time series and thereby represent a challenge for classification and mowing detection.

5.2. Grassland Typology and Perspectives

Previously, a few studies have considered the classification of grassland management practices and intensities through remote sensing, showing promising results but often lacking sufficient representative ground truth data for validation. Using a supervised classification algorithm on RapidEye imagery and a rule-based method to estimate the first mowing date, Franke et al. [30] classified four types of grassland (semi-natural, extensive, intensive, and tilled) with high accuracy on a small study area in Germany. The red-edge vegetation index derived from five RapidEye images was used by Gómez Giménez et al. [32] to retrieve a grassland-use intensity index based on the individual estimation of three factors (mowing, grazing, and fertilization intensity). They obtained promising results for the estimation of grazing and mowing intensities but lacked actual ground truth data for validation.

In this study, the hierarchical categorization based on the classification and the mowing detection allowed to differentiate five types of grassland based on the main management practice (grazing or mowing), the date of the first mowing event, and the mowing frequency. Thanks to the large and regionally representative field dataset, we showed that three classes (pastures, meadows with an early first mowing event, and a late first mowing event) could be differentiated with 79% overall accuracy. The mowing frequency estimation could not be validated because the field campaign was only carried out between April 9th and July 19th, while mowing events occur until the end of October. However, given the high detection accuracy obtained during the study period, we make the hypothesis that the detections remain relatively accurate throughout the season.

While *hay meadows* could be further differentiated through the mowing detection, *pastures* were not further categorized. In a recent study with a similar hierarchical categorization approach, pastures and mown grasslands were differentiated based on biomass productivity and both classes were then subdivided into three management levels based on the exploitation (i.e., harvest) frequency [29]. Both the biomass productivity and the exploitation frequency were retrieved through the detection of significant drops in Landsat NDVI time series, considering the cumulative change and the count of drops, respectively. While this approach showed consistent results with regional statistics and georeferenced land-use data, the land-use intensity levels of both classes could not be validated due to a lack of ground truth data. Moreover, the timing of the first exploitation activity should be considered in addition to the exploitation frequency as it is a major factor of grassland-use intensity and has an influence on their ecological value [57,58].

We showed that the retrieval of homogeneously managed grassland patches and the identification of pastures greatly improved the precision of the mowing detection and allowed to classify five grassland types with high accuracy. These management units could further serve as a baseline to retrieve other grassland characteristics and study their relationships with biodiversity and ecology. The method developed in this study should be further tested in different conditions to be able to extend it over larger areas and transfer it to other seasons to classify grasslands at the landscape level [58,59] and study inter-annual variations [20] to contribute to ecological habitat monitoring.

6. Conclusions

Several studies have shown the great potential of remote sensing for grassland monitoring. In particular, the most recent developments in automated mowing detection methods allow estimating mowing dates and frequencies with high accuracy. In this study, we built on previous achievements to produce a thematically improved grassland classification, differentiating five management classes. First, a pixel-based classification using LAI time series differentiated *pastures* from *hay meadows* with an overall accuracy of 88%. An object-based mowing detection method using the Sentinel-1 coherence and Sentinel-2 NDVI was then applied to further differentiate *hay meadows* by the timing and frequency of the mowing events. The pixel-based approach and the strict grassland mask built for the classification allowed to retrieve homogeneous grassland management units. Moreover, the preliminary identification of grazed grasslands reduced the number of false positives due to the confusion between the grazing and mowing activities during the mowing detection. The hierarchical classification method differentiated pastures and the meadows with an early first mowing event and a late first mowing event with an overall accuracy of 79%. The retrieved management practices could be combined with other factors and environmental context for further grassland characterization to contribute to ecological habitat monitoring.

Author Contributions: Conceptualization, M.D.V., J.R. and P.D.; methodology, M.D.V.; supervision, J.R. and P.D.; validation, M.D.V.; writing—original draft, M.D.V.; writing—review and editing, M.D.V., J.R. and P.D. All authors have read and agreed to the published version of the manuscript.

Funding: This research was funded by the Fédération Wallonie-Bruxelles in the frame of the contribution of Belgium to Lifewatch-ERIC, the European Research Infrastructure Consortium for biodiversity and ecosystem research.

Conflicts of Interest: The authors declare no conflict of interest.

References

1. O'Mara, F.P. The role of grasslands in food security and climate change. *Ann. Bot.* **2012**, *110*, 1263–1270. [CrossRef] [PubMed]
2. Herrero, M.; Havlík, P.; Valin, H.; Notenbaert, A.; Rufino, M.C.; Thornton, P.K.; Blümmel, M.; Weiss, F.; Grace, D.; Obersteiner, M. Biomass use, production, feed efficiencies, and greenhouse gas emissions from global livestock systems. *Proc. Natl. Acad. Sci. USA* **2013**, *110*, 20888–20893. [CrossRef]
3. Bengtsson, J.; Bullock, J.; Egoh, B.; Everson, C.; Everson, T.; O'Connor, T.; O'Farrell, P.; Smith, H.; Lindborg, R. Grasslands—More important for ecosystem services than you might think. *Ecosphere* **2019**, *10*, e02582. [CrossRef]
4. Chang, J.; Ciais, P.; Gasser, T.; Smith, P.; Herrero, M.; Havlík, P.; Obersteiner, M.; Guenet, B.; Goll, D.S.; Li, W.; et al. Climate warming from managed grasslands cancels the cooling effect of carbon sinks in sparsely grazed and natural grasslands. *Nat. Commun.* **2021**, *12*, 1–10. [CrossRef]
5. Zhao, Y.; Liu, Z.; Wu, J. Grassland ecosystem services: A systematic review of research advances and future directions. *Landsc. Ecol.* **2020**, *35*, 793–814. [CrossRef]
6. Pärtel, M.; Bruun, H.H.; Sammul, M. Biodiversity in temperate European grasslands: Origin and conservation. In *Grassland Science in Europe*; Grassland Science in Europe: Tartu, Estonia, 2005; pp. 1–14.
7. Zeller, U.; Starik, N.; Göttert, T. Biodiversity, land use and ecosystem services—An organismic and comparative approach to different geographical regions. *Glob. Ecol. Conserv.* **2017**, *10*, 114–125. [CrossRef]
8. Hansen, M.C.; Defries, R.S.; Townshend, J.R.G.; Sohlberg, R. Global land cover classification at 1 km spatial resolution using a classification tree approach. *Int. J. Remote Sens.* **2000**, *21*, 1331–1364. [CrossRef]
9. Arino, O.; Ramos Perez, J.; Kalogirou, V.; Van Bogaert, E.; Defourny, P.; Bontemps, S. *Global Land Cover Map for 2009 (GlobCover 2009)*; European Space Agency (ESA) and Université catholique de Louvain (UCL): Louvain-la-Neuve, Belgium, 2012.
10. Tsendbazar, N.; Herold, M.; Mayaux, P.; Achard, F.; Kirches, G.; Brockmann, C.; Boettcher, M.; Lamarche, C.; Bontemps, S.; Defourny, P. *CCI Land Cover Product Validation and Inter-Comparison Report*; Technical Report; Université catholique de Louvain (UCL)—Geomatics: Louvain-la-Neuve, Belgium, 2014.
11. Grigulis, K.; Lavorel, S.; Krainer, U.; Legay, N.; Baxendale, C.; Dumont, M.; Kastl, E.; Arnoldi, C.; Bardgett, R.D.; Poly, F.; et al. Relative contributions of plant traits and soil microbial properties to mountain grassland ecosystem services. *J. Ecol.* **2013**, *101*, 47–57. [CrossRef]
12. Abdalla, M.; Hastings, A.; Chadwick, D.; Jones, D.L.; Evans, C.; Jones, M.B.; Rees, R.; Smith, P. Critical review of the impacts of grazing intensity on soil organic carbon storage and other soil quality indicators in extensively managed grasslands. *Agric. Ecosyst. Environ.* **2018**, *253*, 62–81. [CrossRef]

13. Klein, N.; Theux, C.; Arlettaz, R.; Jacot, A.; Pradervand, J.N. Modeling the effects of grassland management intensity on biodiversity. *Ecol. Evol.* **2020**, *10*, 13518–13529. [CrossRef]
14. Andersen, E.; Elbersen, B.; Godeschalk, F.; Verhoog, D. Farm management indicators and farm typologies as a basis for assessments in a changing policy environment. *J. Environ. Manag.* **2007**, *82*, 353–362. [CrossRef] [PubMed]
15. Hudewenz, A.; Klein, A.M.; Scherber, C.; Stanke, L.; Tscharntke, T.; Vogel, A.; Weigelt, A.; Weisser, W.W.; Ebeling, A. Herbivore and pollinator responses to grassland management intensity along experimental changes in plant species richness. *Biol. Conserv.* **2012**, *150*, 42–52. [CrossRef]
16. Chisté, M.N.; Mody, K.; Gossner, M.M.; Simons, N.K.; Köhler, G.; Weisser, W.W.; Blüthgen, N. Losers, winners, and opportunists: How grassland land-use intensity affects orthopteran communities. *Ecosphere* **2016**, *7*, e01545. [CrossRef]
17. Busch, V.; Klaus, V.H.; Schäfer, D.; Prati, D.; Boch, S.; Müller, J.; Chisté, M.; Mody, K.; Blüthgen, N.; Fischer, M.; et al. Will I stay or will I go? Plant species-specific response and tolerance to high land-use intensity in temperate grassland ecosystems. *J. Veg. Sci.* **2019**, *30*, 674–686. [CrossRef]
18. Ekroos, J.; Kleijn, D.; Batáry, P.; Albrecht, M.; Báldi, A.; Blüthgen, N.; Knop, E.; Kovács-Hostyánszki, A.; Smith, H.G. High land-use intensity in grasslands constrains wild bee species richness in Europe. *Biol. Conserv.* **2020**, *241*, 108255. [CrossRef]
19. Clough, Y.; Ekroos, J.; Báldi, A.; Batáry, P.; Bommarco, R.; Gross, N.; Holzschuh, A.; Hopfenmüller, S.; Knop, E.; Kuussaari, M.; et al. Density of insect-pollinated grassland plants decreases with increasing surrounding land-use intensity. *Ecol. Lett.* **2014**, *17*, 1168–1177. [CrossRef]
20. Allan, E.; Bossdorf, O.; Dormann, C.F.; Prati, D.; Gossner, M.M.; Tscharntke, T.; Blüthgen, N.; Bellach, M.; Birkhofer, K.; Boch, S.; et al. Interannual variation in land-use intensity enhances grassland multidiversity. *Proc. Natl. Acad. Sci. USA* **2014**, *111*, 308–313. [CrossRef]
21. Dufrêne, M.; Delescaille, L.M. La Typologie WalEUNIS des Biotopes Wallons, Version 1.0. 2005. Available online: http://biodiversite.wallonie.be (accessed on 23 December 2022).
22. Blüthgen, N.; Dormann, C.F.; Prati, D.; Klaus, V.H.; Kleinebecker, T.; Hölzel, N.; Alt, F.; Boch, S.; Gockel, S.; Hemp, A.; et al. A quantitative index of land-use intensity in grasslands: Integrating mowing, grazing and fertilization. *Basic Appl. Ecol.* **2012**, *13*, 207–220. [CrossRef]
23. Tonn, B.; Bausson, C.; Ten Berge, H.; Buchmann, N.; Bufe, C.; Eggers, S.; Fernández-Rebollo, P.; Forster-Brown, C.; Hiron, M.; Klaus, V.; et al. A management-based typology for European permanent grasslands. In Proceedings of the 28th General Meeting of European Grassland Federation, Online, 19–21 October 2020; Volume 25, pp. 412–414.
24. Ali, I.; Cawkwell, F.; Dwyer, E.; Barrett, B.; Green, S. Satellite remote sensing of grasslands: From observation to management. *J. Plant Ecol.* **2016**, *9*, 649–671. [CrossRef]
25. Reinermann, S.; Asam, S.; Kuenzer, C. Remote Sensing of Grassland Production and Management—A Review. *Remote Sens.* **2020**, *12*, 1949. [CrossRef]
26. Rapinel, S.; Mony, C.; Lecoq, L.; Clement, B.; Thomas, A.; Hubert-Moy, L. Evaluation of Sentinel-2 time-series for mapping floodplain grassland plant communities. *Remote Sens. Environ.* **2019**, *223*, 115–129. [CrossRef]
27. Fazzini, P.; De Felice Proia, G.; Adamo, M.; Blonda, P.; Petracchini, F.; Forte, L.; Tarantino, C. Sentinel-2 Remote Sensed Image Classification with Patchwise Trained ConvNets for Grassland Habitat Discrimination. *Remote Sens.* **2021**, *13*, 2276. [CrossRef]
28. Kaasiku, T.; Praks, J.; Jakobson, K.; Rannap, R. Radar remote sensing as a novel tool to assess the performance of an agri-environment scheme in coastal grasslands. *Basic Appl. Ecol.* **2021**, *56*, 464–475. [CrossRef]
29. Stumpf, F.; Schneider, M.K.; Keller, A.; Mayr, A.; Rentschler, T.; Meuli, R.G.; Schaepman, M.; Liebisch, F. Spatial monitoring of grassland management using multi-temporal satellite imagery. *Ecol. Indic.* **2020**, *113*, 106201. [CrossRef]
30. Franke, J.; Keuck, V.; Siegert, F. Assessment of grassland use intensity by remote sensing to support conservation schemes. *J. Nat. Conserv.* **2012**, *20*, 125–134. [CrossRef]
31. Asam, S.; Klein, D.; Dech, S. Estimation of grassland use intensities based on high spatial resolution LAI time series. *ISPRS—Int. Arch. Photogramm. Remote. Sens. Spat. Inf. Sci.* **2015**, *XL-7/W3*, 285–291. [CrossRef]
32. Gómez Giménez, M.; de Jong, R.; Della Peruta, R.; Keller, A.; Schaepman, M.E. Determination of grassland use intensity based on multi-temporal remote sensing data and ecological indicators. *Remote Sens. Environ.* **2017**, *198*, 126–139. [CrossRef]
33. Estel, S.; Mader, S.; Levers, C.; Verburg, P.H.; Baumann, M.; Kuemmerle, T. Combining satellite data and agricultural statistics to map grassland management intensity in Europe. *Environ. Res. Lett.* **2018**, *13*, 074020. [CrossRef]
34. Hardy, T.; Kooistra, L.; Domingues Franceschini, M.; Richter, S.; Vonk, E.; van den Eertwegh, G.; van Deijl, D. Sen2Grass: A Cloud-Based Solution to Generate Field-Specific Grassland Information Derived from Sentinel-2 Imagery. *AgriEngineering* **2021**, *3*, 118–137. [CrossRef]
35. Savage, J.; Woodcock, B.A.; Bullock, J.M.; Nowakowski, M.; Tallowin, J.R.; Pywell, R.F. Management to Support Multiple Ecosystem Services from Productive Grasslands. *Sustainability* **2021**, *13*, 6263. [CrossRef]
36. Van Vooren, L.; Reubens, B.; Broekx, S.; Reheul, D.; Verheyen, K. Assessing the impact of grassland management extensification in temperate areas on multiple ecosystem services and biodiversity. *Agric. Ecosyst. Environ.* **2018**, *267*, 201–212. [CrossRef]
37. Kolecka, N.; Ginzler, C.; Pazur, R.; Price, B.; Verburg, P.H. Regional Scale Mapping of Grassland Mowing Frequency with Sentinel-2 Time Series. *Remote Sens.* **2018**, *10*, 1221. [CrossRef]

38. Schwieder, M.; Wesemeyer, M.; Frantz, D.; Pfoch, K.; Erasmi, S.; Pickert, J.; Nendel, C.; Hostert, P. Mapping grassland mowing events across Germany based on combined Sentinel-2 and Landsat 8 time series. *Remote Sens. Environ.* **2022**, *269*, 112795. [CrossRef]
39. Voormansik, K.; Zalite, K.; Sünter, I.; Tamm, T.; Koppel, K.; Verro, T.; Brauns, A.; Jakovels, D.; Praks, J. Separability of Mowing and Ploughing Events on Short Temporal Baseline Sentinel-1 Coherence Time Series. *Remote Sens.* **2020**, *12*, 3784. [CrossRef]
40. De Vroey, M.; Radoux, J.; Defourny, P. Grassland Mowing Detection Using Sentinel-1 Time Series: Potential and Limitations. *Remote Sens.* **2021**, *13*, 348. [CrossRef]
41. Lobert, F.; Holtgrave, A.K.; Schwieder, M.; Pause, M.; Vogt, J.; Gocht, A.; Erasmi, S. Mowing event detection in permanent grasslands: Systematic evaluation of input features from Sentinel-1, Sentinel-2, and Landsat 8 time series. *Remote Sens. Environ.* **2021**, *267*, 112751. [CrossRef]
42. De Vroey, M.; de Vendictis, L.; Zavagli, M.; Bontemps, S.; Heymans, D.; Radoux, J.; Koetz, B.; Defourny, P. Mowing detection using Sentinel-1 and Sentinel-2 time series for large scale grassland monitoring. *Remote Sens. Environ.* **2022**, *280*, 113145. [CrossRef]
43. Tamm, T.; Zalite, K.; Voormansik, K.; Talgre, L. Relating Sentinel-1 Interferometric Coherence to Mowing Events on Grasslands. *Remote Sens.* **2016**, *8*, 802. [CrossRef]
44. Griffiths, P.; Nendel, C.; Pickert, J.; Hostert, P. Towards national-scale characterization of grassland use intensity from integrated Sentinel-2 and Landsat time series. *Remote Sens. Environ.* **2020**, *238*, 111124. [CrossRef]
45. Zheng, J.; Li, F.; Du, X. Using Red Edge Position Shift to Monitor Grassland Grazing Intensity in Inner Mongolia. *J. Indian Soc. Remote Sens.* **2018**, *46*, 81–88. [CrossRef]
46. Statbel. (Direction Générale Statistique–Statistics Belgium)–Service Public Fédéral Economie, P.M.E., Classes Moyennes et Energie. Chiffres Clés de l'Agriculture. 2020. Available online: https://statbel.fgov.be/sites/default/files/files/documents/landbouw (accessed on 23 July 2021).
47. ESA. Sentinel Application Platform (snap). v6.0. Available online: http://step.esa.int (accessed on 23 December 2022).
48. Zhu, Z.; Woodcock, C.E. Object-based cloud and cloud shadow detection in Landsat imagery. *Remote Sens. Environ.* **2012**, *118*, 83–94. [CrossRef]
49. Baetens, L.; Desjardins, C.; Hagolle, O. Validation of copernicus Sentinel-2 cloud masks obtained from MAJA, Sen2Cor, and FMask processors using reference cloud masks generated with a supervised active learning procedure. *Remote Sens.* **2019**, *11*, 433. [CrossRef]
50. Weiss, M.; Baret, F. Evaluation of canopy biophysical variable retrieval performances from the accumulation of large swath satellite data. *Remote Sens. Environ.* **1999**, *70*, 293–306. [CrossRef]
51. Inglada, J. OTB Gapfilling, a Temporal Gapfilling for Image Time Series Library. 2016. Available online: https://www.orfeo-toolbox.org/CookBook/Applications/app_ImageTimeSeriesGapFilling.html (accessed on 23 December 2022).
52. Grizonnet, M.; Michel, J.; Poughon, V.; Inglada, J.; Savinaud, M.; Cresson, R. Orfeo ToolBox: Open source processing of remote sensing images. *Open Geospat. Data Softw. Stand.* **2017**, *2*, 1–8. [CrossRef]
53. Inglada, J.; Arias, M.; Tardy, B.; Hagolle, O.; Valero, S.; Morin, D.; Dedieu, G.; Sepulcre, G.; Bontemps, S.; Defourny, P.; et al. Assessment of an operational system for crop type map production using high temporal and spatial resolution satellite optical imagery. *Remote Sens.* **2015**, *7*, 12356–12379. [CrossRef]
54. Radoux, J. LifeWatch Land Cover Product. 2019. Available online: https://maps.elie.ucl.ac.be/lifewatch/ecotopes.html?lang=en (accessed on 23 December 2022).
55. Bontemps, S.; Bajec, K.; Cara, C.; Defourny, P.; De Vendictis, L.; Heymans, D.; Kucera, L.; Malcorps, P.; Milcinski, G.; Nicola, L.; et al. Sen4CAP—Sentinels for Common Agricultural Policy. *Syst. Softw. User Manual. Sen4CAP_SUM_v1* **2022**, *2*. Available online: http://esa-sen4cap.org/sites/default/files/Sen4CAP_SUM_v3.1.pdf (accessed on 23 December 2022).
56. Dusseux, P.; Vertès, F.; Corpetti, T.; Corgne, S.; Hubert-Moy, L. Agricultural practices in grasslands detected by spatial remote sensing. *Environ. Monit. Assess.* **2014**, *186*, 8249–8265. [CrossRef]
57. Humbert, J.Y.; Pellet, J.; Buri, P.; Arlettaz, R. Does delaying the first mowing date benefit biodiversity in meadowland? *Environ. Evid.* **2012**, *1*, 1–13. [CrossRef]
58. Johansen, L.; Westin, A.; Wehn, S.; Iuga, A.; Ivascu, C.M.; Kallioniemi, E.; Lennartsson, T. Traditional semi-natural grassland management with heterogeneous mowing times enhances flower resources for pollinators in agricultural landscapes. *Glob. Ecol. Conserv.* **2019**, *18*, e00619. [CrossRef]
59. Shahan, J.L.; Goodwin, B.J.; Rundquist, B.C. Grassland songbird occurrence on remnant prairie patches is primarily determined by landscape characteristics. *Landsc. Ecol.* **2017**, *32*, 971–988. [CrossRef]